Received: 12 July 2018 | Revised: 30 January 2019 | Accepted: 25 February 2019

DOI: 10.1002/pip.3130

EU PVSEC PAPER

WILEY PROGRESS IN PHOTOVOLTAICS

Prediction of local temperature-dependent performance of silicon solar cells

Rebekka Eberle[1] | Andreas Fell[1] | Sven Mägdefessel[2] | Florian Schindler[1] | Martin C. Schubert[1]

[1] Fraunhofer Institute for Solar Energy Systems ISE, Heidenhofstraße 2, Freiburg 79110, Germany

[2] University Freiburg, Hermann-Herder-Straße 3a, Freiburg 79104, Germany

Correspondence
Rebekka Eberle, Fraunhofer Institute for Solar Energy Systems ISE, Heidenhofstraße 2, Freiburg 79110, Germany.
Email: rebekka.eberle@ise.fraunhofer.de

Funding information
Bundesministerium für Wirtschaft und Energie; PROGNOSIS, Grant/Award Number: 0324160

Abstract

In this study, we present a method to predict the local temperature-dependent performance of silicon solar cells from wafer lifetime images, which enables local investigation of silicon solar cell parameters under realistic operation conditions. The multicrystalline silicon wafers investigated underwent high-temperature steps equivalent to emitter diffusion and contact firing for the production of a passivated emitter and rear cell (PERC) solar cell. Injection and temperature-dependent lifetime images, gathered by calibrated photoluminescence (PL) imaging, are combined with numerical cell device simulations using Quokka3. Hereby, the spatially resolved open-circuit voltage V_{OC}, short-circuit current density j_{SC}, fill factor *FF*, and the efficiency η of a virtual solar cell based on the characterized material are predicted for various temperatures. These data are used to compute temperature coefficients of the aforementioned cell parameters. Our predictions are validated by a comparison with measurement results of cells made from sister wafers, which are analyzed globally and spatially resolved via PL imaging, Lock-in Thermography, and Light-Beam-Induced-Current measurements. We observed a lower temperature sensitivity of IV parameters in dislocation clusters despite of expecting high changes with temperature, which might be explainable by Shockley-Read-Hall (SRH) recombination of impurities like interstitial chromium.

KEYWORDS

ELBA, LBIC, lock-in thermography, photoluminescence, silicon, simulation, solar cells, spatial resolution, temperature sensitivity

1 | INTRODUCTION

Solar cells are typically analyzed at predefined measurement parameters, the so-called "Standard Testing Conditions" (STC), with a temperature of 25°C and an irradiation intensity equivalent to 1 sun at AM 1.5 G with 1000 W/m^2.[1,2] These standards are chosen for an easy worldwide comparison of cells and modules. Cell qualities can be compared via *short-circuit current density* j_{SC}, *open-circuit voltage* V_{OC}, *fill factor FF*, and *efficiency* η in a simple matter.

However, measurements at STC do not reflect the real conditions in which solar cells operate primarily: Clouds and varying solar altitude lead to significant changes of illumination intensity and spectrum. This work deals with the impact of varying cell temperature, which may increase in normal operation to values of up to 70°C.[3] The cell temperature has a significant and rather complex influence on the output characteristics: With increasing temperature j_{sc} increases, as the decrease of *band gap energy* E_g leads to a higher absorption of low energetic photons, and therefore, more free charge carriers are

generated.[4] The fill factor *FF* is influenced by an ideal fill factor FF_0, reduced by injection-dependent lifetime of excess charge carriers τ, and a cell's series resistance R_S.[5-7] *FF* is usually decreasing with temperature as FF_0 decreases and R_S increases because of stronger-contact resistance. However, the temperature sensitivity of τ is more complex and may lead to nontrivial temperature dependence of *FF*. Besides *FF* and j_{SC}, the temperature dependence of V_{OC} has the highest impact on a cell's temperature-dependent behavior[4]: V_{OC} has a negative temperature sensitivity as it decreases with temperature because of increasing intrinsic charge carrier density, which leads to weakened splitting of the quasi-fermi levels.

The global temperature-dependent behavior of solar cells was already studied in detail in the last decades, and general equations for calculation of V_{OC}, *FF*, and other parameters are derived.[3,5,8-12] However, only very few studies dealt with the characterization of solar cell temperature sensitivity in a spatial resolution,[13,14] showed that it is possible to map the local behavior of cells with temperature to study the performance of various regions of silicon material with varying quality, eg, for multicrystalline silicon samples.

In this work, we enhance the "Efficiency Limiting Bulk recombination Analysis" (ELBA)[15] approach for material characterization by including temperature dependence into the analysis. ELBA is an established standard procedure to analyze the spatially resolved efficiency potential of silicon wafers at an early production stage. Injection-dependent photoluminescence (PL) images of silicon wafers calibrated to lifetime via modulated PL at varying temperatures in combination with cell device simulations are used to predict the performance of a solar cell made of this material; this enables an analysis of temperature sensitivity before cell production to predict the influence in particular of material with inhomogeneous quality like multicrystalline silicon.

2 | MODELLING

In this study, we enhance the *ELBA*[15,16] approach for material characterization for the analysis of temperature dependence. The *ELBA* approach is an established standard procedure to analyze the local and global efficiency potential of silicon wafers before metallization. It calculates the efficiency of a solar cell assuming that the local quality of the material is true for every pixel of the analysis. Its principles and improvements are explained in the following:

Spatially resolved and injection-dependent lifetime maps are gained via calibrated PL imaging for passivated silicon wafers after all cell technology specific temperature steps.[17] An example of a lifetime map gathered at STC of 1 sun and 25°C is depicted in Figure 1 A. A particular solar cell concept, in this work a Fraunhofer ISE Passivated Emitter and Rear Cell (PERC) design similar to industry standard, is then used for simulation. We establish for this cell design a complete set of electro-optical device properties, except bulk lifetime, which is directly measured for the analyzed samples. The device simulation is first done for a broad range of τ values resulting in a look-up table for excess charge carrier density Δn, V_{OC}, j_{SC}, *FF*, and η and is then applied to the actually measured injection-dependent lifetime maps. In an iterative procedure, Δn and the bulk lifetime τ_{bulk} for a specific operating point are calculated, and via an interpolation V_{OC}, j_{SC}, *FF*, and η are determined for each pixel. Global values are gathered by averaging according to Isenberg et al.[18]

The main achievement of this work is the enhancement of *ELBA* by temperature-dependent sample characterization and temperature-dependent cell performance prediction: Measurements of effective lifetime are not only conducted at STC but also at various temperatures from 15 to up to 70°C. An *ELBA* analysis is done at all measured temperatures, considering the actual sample temperature for evaluation. The gathered results are fitted with a linear approximation[4,12] to get insight into material related temperature coefficients (*TC*) of solar cells.

To predict reliable solar cell characteristics for various temperatures, the underlying cell device simulations have to take temperature dependence into account. Notably, some fundamental uncertainties in temperature-dependent solar cell modeling still exist.[19]

The device simulation in ELBA is changed from the previously applied software PC1D to Quokka3.[20] By using the "lumped skin" approach based on the conductive boundary model,[21] the near-surface regions ("skins," eg, Back-Surface-Field [BSF] and emitter regions) are defined essentially by the input parameters dark saturation current J_0 and sheet resistance R_{sheet}. While the required number of input parameters is simplified in this approach compared with the more detailed model of the skins as in PC1D, the overall sensitivity to varying bulk lifetime does not change because of its negligible

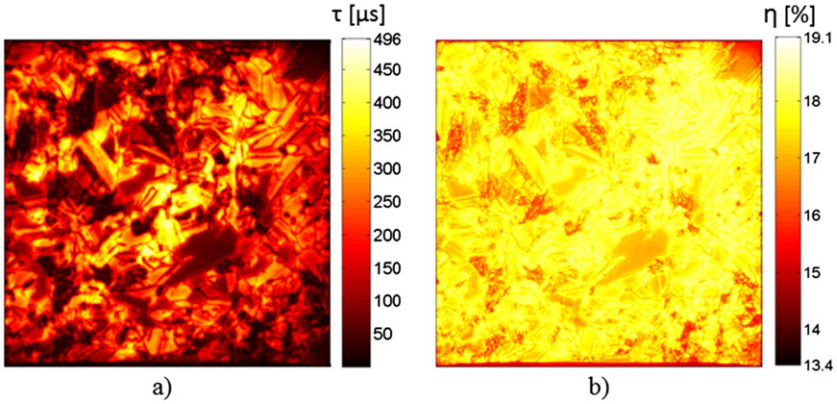

FIGURE 1 A, Carrier lifetime map of a multicrystalline p-type silicon wafer taken at STC temperature of 25°C and monochromatic irradiation at 803 nm with intensity equivalent to approximately 1 sun, B, With Efficiency Limiting Bulk recombination Analysis (ELBA) calculated efficiency map of the same sample at 1 sun and 25°C [Colour figure can be viewed at wileyonlinelibrary.com]

effect on the lumped skin properties. For the temperature dependence of the lumped skin, Quokka3 assumes that J_0/n_i^2 is temperature independent, mainly assuming a temperature-independent effective minority carrier lifetime within those skins. The recombination for measured samples in this study is dominated by the bulk, and there is good agreement between simulation and measurements. Therefore, the used simplification of assuming that J_0/n_i^2 is temperature independent appears suitable for this work. In the bulk region the latest temperature-dependent silicon material models are employed: band gap and density of states and the relation to intrinsic carrier density, by Couderc et al[22]; mobility by Klaasen[23]; band-to-band absorption by Schinke et al.[24]

As it can predict the temperature dependence of the generation current, the lumped parameter optical model of Quokka3 is used in this work,[25] where the light trapping parameters are fitted to match STC-j_{SC}.

Most input parameters for electro-optical device simulation in Quokka3 are mainly gathered by independent measurement. The external series resistance R_S is determined via the difference between measured and simulated internal resistance at each temperature.

3 | EXPERIMENTAL

Samples used in this study are industrial multicrystalline p-type wafers with a thickness of approximately 185 µm and a base resistivity of approximately 1.6 Ωcm. The samples (156 × 156 mm^2) for carrier lifetime measurements underwent high-temperature steps for emitter diffusion and contact firing typical for the standard industrial "Passivated Emitter and Rear Cell" (PERC) concept.[26,27] Then, the diffused layers are etched back, and the wafers are passivated with Al_2O_3 and SiN_x. Sister wafers with similar crystal structure and same base resistivity are used to produce solar cells with PERC at Fraunhofer ISE[28] to compare cell and wafer results: After acidic texturing and the phosphorus emitter diffusion, the passivation of the rear side is done by a stack of plasma-enhanced chemical vapor deposited (PECVD) aluminum oxide Al_2O_3 and SiN_x, the front side by SiN_y. Contacts are applied via screen printing; the front contact is formed with a firing step in a fast firing oven, and contact formation is done via a laser-fired contacts (LFC) process.[28]

A combination of measurement tools are used in this study: PL imaging gains spatially resolved information about silicon lifetime samples, which are irradiated with a 803nm laser, a charge-coupled device (CCD) camera captures PL of the samples, and a stack of long-pass filters with additional 1000 and 1050-nm short-pass filter suppresses detection of reflected laser light and reduces optical blurring. Gathered PL images are calibrated to effective lifetime τ_{eff} with lifetime measurements via harmonically modulated PL.[17] Lifetime images are eventually used for ELBA, and therefore, PL imaging is crucial for efficiency prediction.

To evaluate ELBA results, a comparison with actual measurements of cells made from the same base material is needed, in local as well as spatial resolution. For this purpose, characterization of global cell parameters is done with the measurement system LOANA by PV Tools GmbH,[29] which measures global η, V_{OC}, j_{SC}, and *FF* and reflectance, external quantum efficiency *EQE*, or grid parameters. The local performance of the cells is studied by a Total Cell Analysis (*TCA*).[30] This method combines Coupled-Determination of Dark Saturation Current and Series Resistance (*C-DCR*),[31] a Local-IV analysis of Dark Lock-In Thermography (*DLIT*),[32] and j_{SC} mapping via Spectrally Resolved-Light Beam Induced Current (*SR-LBIC*) measurements[33] to map the spatially resolved η of a solar cell as well as V_{OC}, j_{SC}, and *FF* (for details, see cited literature).

To analyze the temperature-dependent behavior of silicon solar cells and lifetime samples, the aforementioned measurement approaches are enhanced: The measurement chucks are temperature controlled with Peltier elements by which measurements at various temperatures from 15 to 70°C are conducted. For an overview of the various approaches with needed measurements and their characteristics, see Table 1.

4 | RESULTS

4.1 | Prediction of temperature sensitivity

An example of a lifetime map gathered at STC temperature of 25°C and 1-sun irradiation with 803-nm light is shown in Figure 1A. The resulting simulated η for this lifetime sample at 25°C and 1 sun is shown in Figure 1B. For that map up to 20, lifetime-calibrated injection-dependent PL images are combined with a cell simulation with Quokka3. From measurements in the temperature range between 15 and 70°C, local TC are calculated with a linear approximation.

The spatially resolved change in η with temperature is analyzed in Figure 2A. The multicrystalline structure of the characterized sample is still visible in the temperature coefficient map; areas of dislocation

TABLE 1 Comparison of performance parameters η, V_{OC}, j_{SC}, and *FF* predicted with *ELBA*, gathered by global cell measurements and by spatially resolved *TCA* at STC

Method	Sample	Needed Measurements/ software	Output
ELBA prediction	Passivated lifetime sample	-injection dependent PL imaging -Quokka3	Local IV parameters
Global measurement	Finished solarcell	LOANA tool	Global IV parameters
TCA	Finished solarcell	-C-DCR -SR-LBIC -Local-IV	Local IV parameters and series resistance

Abbreviations: C-DCR, Coupled-Determination of Dark Saturation Current and Series Resistance; ELBA, Efficiency Limiting Bulk recombination Analysis; SR-LBIC, Spectrally Resolved-Light Beam Induced Current; STC, Standard Testing Conditions; TCA, Total Cell Analysis.

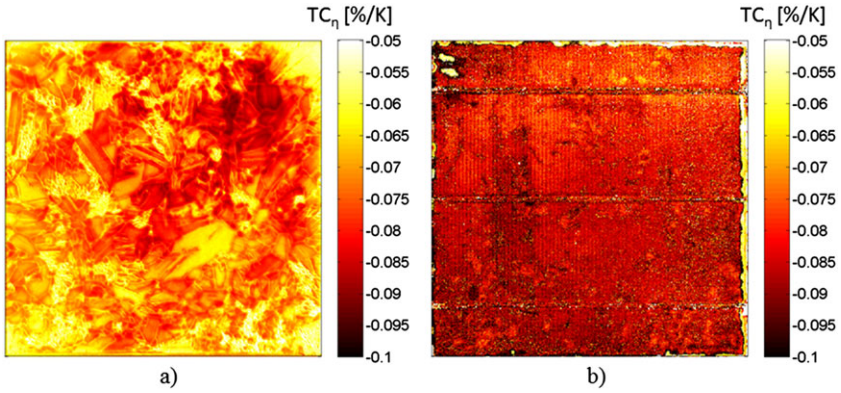

FIGURE 2 A, Temperature-dependent Efficiency Limiting Bulk recombination Analysis (ELBA) results were used to fit local temperature coefficient TCη in spatial resolution, B, Temperature sensitivity of η of a solar cell made from a sister wafer gained from temperature-dependent Total Cell Analysis (TCA) [Colour figure can be viewed at wileyonlinelibrary.com]

clusters can clearly be distinguished from ones with good grains and high τ.

A very similar spatial distribution can be seen for temperature-dependent local V_{OC} in Figure 3A, which commonly dominates the temperature sensitivity of silicon solar cells. V_{OC} shows the same trends in temperature sensitivity for good areas and areas with dislocations as Figure 2A.

To assess the validity of our approach, results are compared with other already established measurement techniques. For this, PERC cells are analyzed with two different characterization methods. The cells are made of sister wafers with very similar crystal structure and material properties, eg, bulk resistivity, as the lifetime samples used for the temperature-dependent *ELBA* analysis.

A global cell characterization via IV measurements with the measurement system *LOANA*,[29] as well as a *TCA*,[30] which gathers local results, is conducted with the produced PERC samples. In Table 2, results are depicted for an irradiation intensity equivalent to 1 sun and a temperature of 25°C: *ELBA* prediction and *TCA* are averaged over the whole sample area (for *ELBA* according to Isenberg et al,[18] for *TCA* j_{SC} arithmetic and V_{OC} square-root harmonic) and compared with global measurement via *LOANA*. The slight overestimation of *FF* by *ELBA* is explained by the simulation neglecting edge effects, nonideal surface recombination, as well as *FF* losses caused by grain-boundary recombination.[34]

Measurements for all shown approaches are not only conducted at STC temperature but also at temperatures from 15 up to 70°C.

TABLE 2 Comparison of performance parameters η, V_{OC}, j_{SC}, and *FF* predicted with *ELBA*, gathered by global cell measurements and by spatially resolved *TCA* at STC

Data Gathered Via	η (%)	V_{OC} (mV)	j_{SC} (mA/cm^2)	FF (%)
ELBA prediction	17.7	640.9	36.17	76.4
Global measurement	17.3	639.2	36.22	74.7
TCA	17.6	642.5	36.55	75.0

Abbreviations: ELBA, Efficiency Limiting Bulk recombination Analysis; STC, Standard Testing Conditions; TCA, Total Cell Analysis.

As for ELBA predictions, for TCA and the global IV characterization, a linear trend for the temperature sensitivity[4] is assumed to fit TC of solar cell parameters. Arithmetically averaged results are shown in Table 3. The satisfactory agreement between all approaches confirms that the assumptions made for cell device simulation in Quokka3 within the improved *ELBA* analysis are sufficient for a temperature sensitivity analysis and efficiency prediction of the investigated wafers.

Besides global results, local cell parameters and their temperature sensitivity can be investigated for their spatial distribution. Figures 2 and 3 show TC of η (Figure 2A) and V_{OC} (Figure 3A) gathered via ELBA. These can be compared with measured local cell results for both parameters (see Figures 2B and 3B, respectively).

Measured TC (Figures 2B and 3B) are distributed more evenly than for ELBA results. We attribute this to lateral conduction of charge

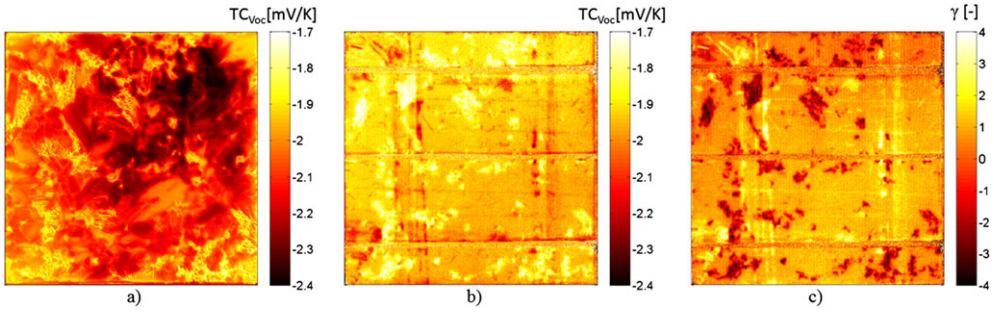

FIGURE 3 A, Spatially resolved TCVoc calculated with Efficiency Limiting Bulk recombination Analysis (ELBA) results, B, Measured spatially resolved TCVoc of a sister Passivated Emitter and Rear Cell (PERC) solar cell, C, γ calculated with Voc map at Standard Testing Conditions (STC) and local TCVoc of PERC cell [Colour figure can be viewed at wileyonlinelibrary.com]

TABLE 3 Comparison of temperature coefficients of η, V_{OC}, j_{SC}, and *FF* predicted with *ELBA*, gathered by global cell measurements and by spatially resolved TCA

Data Gathered Via	TC_η (%/K)	TC_{Voc} (mV/K)	TC_{jsc} (mA/[cm^2·K])	TC_{FF} (%/K)
ELBA prediction	−0.072	−2.10	0.019	−0.11
Global measurement	−0.072	−1.95	0.022	−0.11
TCA	−0.085	−1.93	0.017	−0.14

Abbreviations: ELBA, Efficiency Limiting Bulk recombination Analysis; STC, Standard Testing Conditions; TCA, Total Cell Analysis.

carriers over the whole cell area in the emitter present in the solar cells. Hence, local values for η and V_{OC} do not have the same values but the same local distribution. As for the lifetime samples, a different temperature-dependent behavior for areas of dislocation clusters is distinguishable in the cell measurements. As already shown in previous studies,[13,14] and also obvious from the local results presented here, areas of dislocation clusters with a low initial lifetime are characterized by decreased temperature sensitivity. This leads to a reduced change in IV characteristics with increasing temperature and to a more stable cell and module performance with increasing temperature for samples with high concentration of impurities than expected. The cause of the temperature sensitivity difference in dislocation and high lifetime areas is discussed in the following.

4.2 | Root cause of local TC

According to theory of global temperature-dependent behaviour,[4] TC_{Voc} should increase with higher V_{OC} leading to reduced temperature sensitivity and dominates the overall temperature sensitivity of silicon solar cells. However, in our study dislocation clusters of the multicrystalline silicon samples show the opposite trend: Besides local TC_{Voc} behavior, we found that although we would expect the recombination parameters γ to be increased in areas with low initial *Voc* @STC because of increased recombination,[4] Gamma was even lower and also reached negative values (see Figure 3C). As can be seen in Table 4 by a comparison of actual TC_{Voc} with predicted TC_{Voc} by ELBA, the actual temperature sensitivity of V_{OC} in areas with low initial lifetime and respective low V_{OC} is contradictory to the behavior expected from textbook theory. To analyze the root cause of this anomaly, areas with high initial lifetime (green rectangle in Figure 4 A) and lower material quality (blue rectangle in Figure 4A) are compared, and further investigations are conducted.

TABLE 4 Comparison of temperature coefficients of τ and V_{OC} for whole sample and high (green rectangle in Figure 5A) as well as low lifetime areas (blue rectangle in Figure 5A)

Averaged Values For	$TC_{Voc,Green}$ [mV/K]	$TC_{Voc,ELBA}$ [mV/K]	$TC_{Voc,Cell}$ [mV/K]	TC_τ [µs/K]
Whole sample	−1.93	−2.10	−1.95	0.39
Good area	−1.90	−2.31	−1.92	0
Bad area	−1.99	−1.98	−1.77	0.35

For comparison of V_{OC} in the different areas, results from ELBA, TCA, and calculations with the formula in Green et al[4] ($TC_{Voc,Green}$) are used. Values are averaged harmonically for calculations with τ.

Figure 4A depicts the local TC_τ calculated with lifetime-calibrated PL images taken at approximately 1-sun irradiation intensity showing two different areas, one with negative TC of grains with high initial lifetimes (eg, green rectangle) and a second type of area with positive TC (eg, blue rectangle). This map shows the same spatially resolved pattern as could be seen for ELBA predictions of TC_{Voc} and TC_η. In addition, Figure 4B,C shows temperature and injection level-dependent lifetime for two different areas with low (Figure 4B) and high effective lifetime at STC (Figure 4C); averaged values are listed in Table 4. Especially, the difference in relative change of lifetime at low carrier injection for the good and bad area is significant. ELBA calculates the local efficiency as if the solar cell was made homogeneously out of the material with this local quality, and it correctly predicts the reverse temperature-dependent behavior of dislocation clusters.

One possible cause for the anomaly of temperature-dependent behavior in dislocations could be diffusion of excess charge carriers from good grains into bad areas. To assess this possibility, temperature and injection-dependent lifetime maps, which were used for the ELBA analysis, were corrected for lateral charge carrier diffusion leading to diffusion corrected images.[35] This correction is not applied as a standard feature as diffusion of charge carriers also takes place in solar cells and is therefore important for local efficiency prediction.[14]

Repeated ELBA analysis with diffusion corrected maps delivered the same results as for the original analysis, which implies that charge carrier diffusion can be excluded as cause for improved TC_{Voc} and TC_η of dislocation clusters.

The analyzed multicrystalline sample contains a significant concentration of impurities. This is proven by measurement of local spatially resolved interstitial iron concentration in Figure 5A according to Macdonald et al.[36] However, it was shown in a study of Eberle et al[13] that iron cannot be responsible for the relatively strong increase of lifetime in low-quality areas as a negative TC_τ for various iron concentrations was calculated.

Dislocation clusters are usually characterized by a higher concentration of impurities; these can induce Shockley-Read-Hall (SRH) defects at an energy level in the middle of the band gap and change τ_{eff} significantly.[37,38] To assess this possibility, the injection-dependent *SRH lifetime* τ_{SRH} is simulated for various *trap energy levels* E_t at different temperatures (see Figure 6). Figure 6A shows a calculation of τ_{SRH} for E_t-E_v = 0.374 eV of interstitial iron[39]; there is no significant change in τ_{SRH} at high Δn values and only a weak one for low excess charge carrier densities. Both results confirm the statement of Eberle et al[13] that iron is most probably not responsible for the observed temperature sensitivity in dislocation clusters.

A trap level E_t of 0.265 eV (Figure 6B), which represents chromium-boron pairs at these temperatures,[40] results in a very different behavior: With decreasing Δn, a strong temperature dependence of τ_{SRH} is observed: τ_{SRH} decreases with declining Δn for low to medium temperatures, whereas τ_{SRH} strongly increases for decreasing

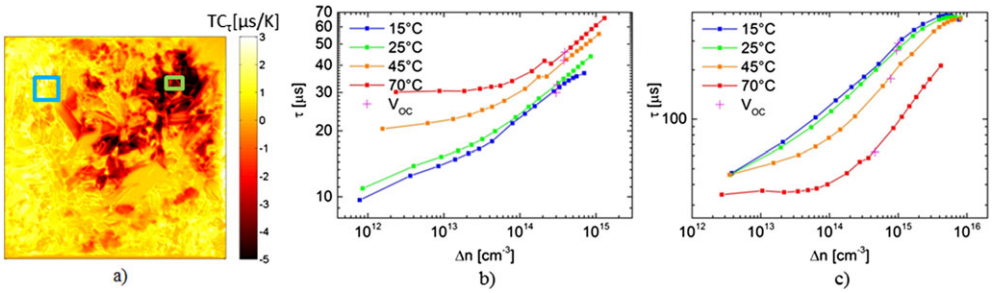

FIGURE 4 A, Spatially resolved temperature coefficient of the excess carrier lifetime assuming linear behavior with temperature, images used for fitting were taken at irradiation intensity equivalent to approximately 1 sun, B, injection level-dependent mean lifetimes at measured temperatures for area with low lifetime (blue rectangle in Figure 4A), C, with high lifetime (green rectangle in Figure 4A) in double logarithmic scaling [Colour figure can be viewed at wileyonlinelibrary.com]

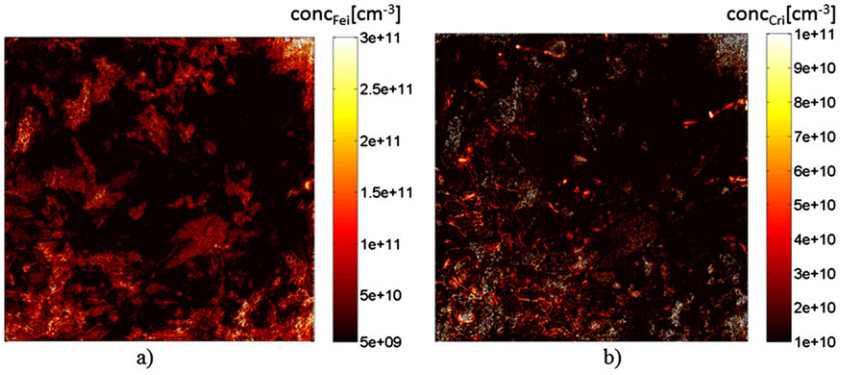

FIGURE 5 Spatially resolved measurement of A, interstitial iron concentration, B, interstitial chromium concentration in investigated lifetime sample [Colour figure can be viewed at wileyonlinelibrary.com]

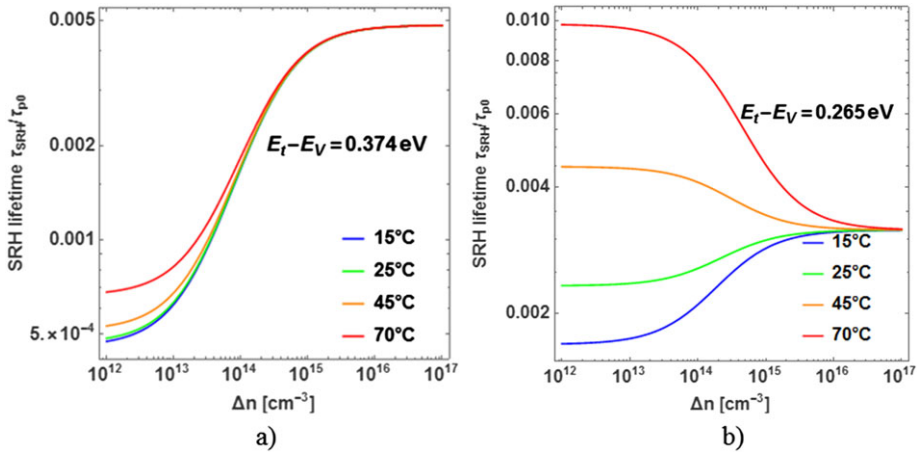

FIGURE 6 Simulated Shockley-Read-Hall (SRH) lifetimes for temperatures from 15 to 70°C and two different energy values of trap levels induced by impurities in the band gap of silicon leading to SRH defects with double logarithmic scaling, for the example of A, interstitial iron impurities, B, chromium boron pairs [Colour figure can be viewed at wileyonlinelibrary.com]

Δn at 70°C. This is only an example for a possible impurity inducing *SRH* recombination with an energy level in the band gap of silicon. Simulations of defects with E_t-E_v of 0.2 to 0.3 eV demonstrate that lifetime strongly increases with temperature from the value at low *Δn* at low temperature to high temperatures and the related increased charge carrier density. This contributes positively to V_{OC}; thus, the decrease of V_{OC} with increasing temperature is reduced, which results in better TC_{Voc}. However, the observed decrease in lifetime at high injection cannot be explained by SRH defects and might stem from a different mechanism as surface recombination, which is still to be investigated.

To assess the possibility of chromium-boron pairs being partly responsible for improved temperature sensitivity in dislocations, a spatially resolved measurement of interstitial chromium Cr_i concentration of the same lifetime sample was conducted;[41] the respective map can be seen in Figure 5B. The sample contains a significant amount of Cr_i,

and its local distribution corresponds to areas of dislocation clusters, which supports our hypothesis.

5 | CONCLUSION

In this work, we report an improved approach for the prediction of solar cell parameters at an early production stage. Temperature and injection-dependent lifetime images are combined with a solar cell device simulation to assess the local and global characteristics of a solar cell and its temperature sensitivity before metallization. The proposed method can be applied to all kinds of silicon samples and can be used to distinguish between effects induced by bulk material and by cell architecture.

As there is reasonable agreement of the predictions with global and local measurements of solar cells made of sister wafers, the analysis approach, as well as the assumptions for electro-optical device modelling, appears to account for all important effects with sufficient accuracy. The local results demonstrate that especially sample regions with low initial lifetime like dislocated areas are characterized by temperature-dependent behavior of which is opposed to expectations from established simpler analytical models, despite expecting an increase γ was found to exhibit negative values in areas of dislocation clusters.

The cause for this anomaly was investigated: Simulations of various *SRH* trap levels exhibit a strong increase in τ_{SRH} for increasing temperatures, which results in increasing τ_{eff} for low excess charge carrier densities. These results imply that impurities leading to *SRH* defects with E_t of 0.2 to 0.3 eV may be part of the complex reason for decreased temperature sensitivity of dislocation clusters.

We conclude from our investigations that the disadvantage of multicrystalline silicon, which is the significantly decreased efficiency caused by a lower local crystal quality, is weakened at higher temperatures as the gap in efficiency between bad and good areas decreases.

ACKNOWLEDGEMENT

We thank Sven Wasmer for providing silicon lifetime and cell samples and detailed sample information for cell simulations. Rebekka Eberle would like to thank the "Studienstiftung des deutschen Volkes" for funding her dissertation project. This work was supported by the Bundesministerium für Wirtschaft und Energie BMWi and by industry partners within the research project PROGNOSIS under contract No. 0324160. The authors are responsible for the content.

ORCID

Rebekka Eberle https://orcid.org/0000-0002-3484-9665
Florian Schindler https://orcid.org/0000-0001-7639-2758

REFERENCES

1. Photovoltaic Deviced: Measurement Principles for Terrestrial Photovoltaic (Pv) Solar Deviced with Reference Spectral Irradiance Data, 3, 2008.
2. Photovoltaic Devices: Standard Reference Climatic Profiles: Spectral Responsitivity, Incidence Angle and Module Operating Temperature Measurements, 4, 2011.
3. Dupré O, Vaillon R, Green MA. A full thermal model for photovoltaic devices. *Sol Energy*. 2016;140:73-82.
4. Green MA, Emery K, Blakers AW. Silicon solar cells with reduced temperature sensitivity. *Electron Lett*. 1982;18(2):97.
5. Dupre O, Vaillon R, Green MA. Experimental assessment of temperature coefficient theories for silicon solar cells. In: *2015 IEEE 42nd Photovoltaic Specialist Conference (PVSC)*. New Orleans, LA; 2015:1-3.
6. Green MA. *Silicon solar cells: Advanced principles & practice*. Sydney: Centre for Photovoltaics devises and systems, University of New South Wales; 1995.
7. Zhao J, Wang A, Robinson SJ, Green MA. Reduced temperature coefficients for recent high-performance silicon solar cells. *Prog Photovolt: Res Appl*. 1994;2(3):221-225.
8. Berthod C, Strandberg R, Yordanov GH, Beyer HG, Odden JO. On the variability of the temperature coefficients of mc-Si solar cells with irradiance. *Energy Procedia*. 2016;92:2-9.
9. Löper P, Pysch D, Richter A, et al. Analysis of the temperature dependence of the open-circuit voltage. *Energy Procedia*. 2012;27:135-142.
10. Green MA. General temperature dependence of solar cell performance and implications for device modelling. *Prog Photovolt: Res Appl*. 2003;11(5):333-340.
11. Singh P, Ravindra NM. Temperature dependence of solar cell performance—an analysis. *Sol Energy Mater Sol Cells*. 2012;101:36-45.
12. Ramspeck K, Plag F, Haas F, Winter S, Metz A. "Temperature coefficients of silicon solar cells," *31st EU PV Conference*, 2015.
13. Eberle R, Haag ST, Geisemeyer I, Padilla M, Schubert MC. Temperature coefficient imaging for silicon solar cells. *IEEE J Photovoltaics*. 2018;8(4):930-936.
14. Eberle R, Kwapil W, Schubert MC. Temperature dependent imaging of solar cell losses. *AIP Conference Proceedings*. 2018;1999:200050–20005.
15. Michl B, Rüdiger M, Giesecke JA, Hermle M, Warta W, Schubert MC. Efficiency limiting bulk recombination in multicrystalline silicon solar cells. *Sol Energy Mater Sol Cells*. 2012;98:441-447.
16. Michl B, Kasemann M, Warta W, Schubert MC. Wafer thickness optimization for silicon solar cells of heterogeneous material quality. *Phys Status Solidi RRL*. 2013;7(11):955-958.
17. Giesecke JA, Schubert MC, Michl B, Schindler F, Warta W. Minority carrier lifetime imaging of silicon wafers calibrated by quasi-steady-state photoluminescence. *Sol Energy Mater Sol Cells*. 2011;95(3):1011-1018.
18. Isenberg J, Dicker J, Warta W. Averaging of laterally inhomogeneous lifetimes for one-dimensional modeling of solar cells. *J Appl Phys*. 2003;94(6):4122-4130.
19. Steinkemper H, Geisemeyer I, Schubert MC, Warta W, Glunz SW. Temperature-dependent modeling of silicon solar cells—Eg, n i, recombination, and VOC. *IEEE J Photovoltaics*. 2017;7(2):450-457.
20. Fell A, Schön J, Schubert MC, Glunz SW. The concept of skins for silicon solar cell modeling. *Sol Energy Mater Sol Cells*. 2017;173:128-133.
21. Brendel R. Modeling solar cells with the dopant-diffused layers treated as conductive boundaries. *Prog Photovolt: Res Appl*. 2012;20(1):31-43.
22. Couderc R, Amara M, Lemiti M. Reassessment of the intrinsic carrier density temperature dependence in crystalline silicon. *J Appl Phys*. 2014;115(9):93705.

23. Klaasen DBM. "A unified mobility model for device simulation—Electron Devices Meeting, 1990. Technical Digest., International," International Technical Digest on Electron Devices, 1990.
24. Schinke C, Bothe K, Christian Peest P, Schmidt J, Brendel R. Uncertainty of the coefficient of band-to-band absorption of crystalline silicon at near-infrared wavelengths. *Appl Phys Lett*. 2014;104(8):81915.
25. Fell A, McIntosh KR, Fong KC. Simplified device simulation of silicon solar cells using a lumped parameter optical model. *IEEE J Photovoltaics*. 2016;6(3):611-616.
26. Blakers AW, Wang A, Milne AM, Zhao J, Green MA. 22.8% efficient silicon solar cell. *Appl Phys Lett*. 1989;55(13):1363-1365.
27. Green MA. The passivated emitter and rear cell (PERC): from conception to mass production. *Sol Energy Mater Sol Cells*. 2015;143:190-197.
28. Wasmer S, Greulich J, Hoffler H, et al. Impact of material and process variations on the distribution of multicrystalline silicon PERC cell efficiencies. *IEEE J Photovoltaics*. 2017;7(1):118-128.
29. "pv-tools GmbH," http://www.pv-tools.de/.
30. Michl B, Padilla M, Geisemeyer I, et al. Imaging techniques for quantitative silicon material and solar cell analysis. *IEEE J Photovoltaics*. 2014;4(6):1502-1510.
31. Glatthaar M, Haunschild J, Kasemann M, Giesecke J, Warta W, Rein S. Spatially resolved determination of dark saturation current and series resistance of silicon solar cells. *Phys Stat Sol (RRL)*. 2010;4(1–2):13-15.
32. Breitenstein O. Nondestructive local analysis of current–voltage characteristics of solar cells by lock-in thermography. *Sol Energy Mater Sol Cells*. 2011;95(10):2933-2936.
33. Padilla M, Michl B, Thaidigsmann B, Warta W, Schubert MC. Short-circuit current density mapping for solar cells. *Sol Energy Mater Sol Cells*. 2014;120:282-288.
34. Schindler F, Fell A, Müller R, et al. Towards the efficiency limits of multicrystalline silicon solar cells. *Sol Energy Mater Sol Cells*. 2018;185:198-204.
35. Phang SP, Sio HC, Macdonald D. Carrier de-smearing of photoluminescence images on silicon wafers using the continuity equation. *Appl Phys Lett*. 2013;103(19):192112.
36. Macdonald D, Tan J, Trupke T. Imaging interstitial iron concentrations in boron-doped crystalline silicon using photoluminescence. *J Appl Phys*. 2008;103(7):73710.
37. Shockley W, Read WT Jr. Statistics of the Recombinations of holes and electrons. *Phys Ther Rev*. 1952;87(5):835-842.
38. Hall RN. Electron-hole recombination in germanium. *Phys Rev*. 1952;87(2):387.
39. Istratov AA, Hieslmair H, Weber ER. Iron and its complexes in silicon. *Appl Phys Mater Sci Process*. 1999;69(1):13-44.
40. Sun C, Rougieux FE, Macdonald D. Reassessment of the recombination parameters of chromium in n- and p-type crystalline silicon and chromium-boron pairs in p-type crystalline silicon. *J Appl Phys*. 2014;115(21):214907.
41. Habenicht H, Schubert MC, Warta W. Imaging of chromium point defects in p-type silicon. *J Appl Phys*. 2010;108(3):34909.

How to cite this article: Eberle R, Fell A, Mägdefessel S, Schindler F, Schubert MC. Prediction of local temperature-dependent performance of silicon solar cells. *Prog Photovolt Res Appl*. 2019;1–8. https://doi.org/10.1002/pip.3130